Generation and Stability of Zonal Flows in Ion-Temperature-Gradient Mode Turbulence

B. N. Rogers,[1] W. Dorland,[1] and M. Kotschenreuther[2]
[1]*Institute for Plasma Research, University of Maryland, College Park, Maryland, 20742*
[2]*Institute for Fusion Studies, University of Texas, Austin, Texas, 78704*
(Received 18 August 2000)

We address the mechanisms underlying zonal flow generation and stability in turbulent systems driven by the electrostatic ion-temperature-gradient (ITG) mode. In the case of zonal flow stability, we show the poloidal flows typical of numerical simulations become unstable when they exceed a critical level. Near marginal stability of the linear ITG mode, the system can generate zonal flows that are sufficiently weak to remain stable and sufficiently strong to suppress the linear ITG mode. This stable region corresponds to the parameter regime of the nonlinear Dimits up-shift.

PACS numbers: 52.35.Ra, 52.35.Kt, 52.65.Ff

Numerical simulations of ion-temperature-gradient (ITG) driven modes in magnetically confined fusion plasmas indicate that poloidal $\mathbf{E} \times \mathbf{B}$ flows, spontaneously generated by the nonlinear dynamics, play a central role in regulating the saturation level of the turbulence and the resulting cross-field heat transport (see, e.g., [1,2]). This is strikingly evident in simulations near marginally stable conditions, in which the sheared flows generated by the system virtually suppress all transport, and lead to an effective nonlinear up-shift of the critical ITG mode instability gradient [3] (the so-called Dimits shift). We address here, in the context of the electrostatic ITG system, two fundamental questions regarding the physics of these sheared poloidal (or "zonal") flows. First, what is the mechanism by which these flows are generated? Second, under what conditions are these flows stable? In the course of our study of the second issue, we reach a new understanding of the dynamics underlying the nonlinear Dimits shift.

To gain insight into the generation of zonal flows by ITG modes, we consider a nonlinear gyrokinetic flux tube simulation near the onset of turbulent saturation. During this phase, a burst of zonal flow growth is observed that is qualitatively similar to (but more extreme than) bursts that are observed throughout the turbulent phase. Starting the simulation from small perturbations, a dominant (primary) linear ITG mode emerges in the linear phase. Figures 1(a) and 1(b) show the squared, field-line-averaged electric potential $|\phi_l|^2$ [Fig. 1(a), dotted line] and growth rate γ_l [Fig. 1(b), dotted line] of this linear mode as a function of time, with $\phi = e\phi_{\rm phys}R/(\rho_{se}T_{e0})$, $\rho_{se} = c_{se}/\Omega_{ci}$, $c_{se} = \sqrt{T_{e0}/m_i}$, $t = t_{\rm phys}c_{se}/R$, $\gamma_l = \gamma_{l,\rm phys}R/c_{se}$. The parameters in the simulation are $R/L_T = 6.9$, $R/L_n = 2.2$, $T_i/T_e = 1$, $\hat{s} = 0.8$, and $r/R = 0.167$. For these parameters the dominant linear mode produces the usual pattern of radial streamers at a well-defined poloidal wave number: $k_y = 0.3$ and $k_x = 0$, where x, y are flux tube radial and poloidal coordinates [4]. The other curves in Fig. 1(a) show the amplitudes of zonal flow modes ($k_x \neq 0, k_y = 0$) in the simulation. These modes are driven by two distinct mechanisms. The first zonal mode to emerge is the lowest k_x harmonic in the system ($k_x = 0.1$, dashed line), and is initially driven by the beating of the dominant linear mode with another linearly unstable ITG mode (not shown) at $k_x = 0.1$, $k_y = -0.3$. This mode, despite its relatively large amplitude in the turbulent phase, leads to weak shearing $k_x^2\phi$ compared to that produced by higher k_x zonal modes in the system. The higher k_x zonal modes, which generate the most important shear flows for the typical parameters we have examined, arise from a different mechanism, and exhibit a k_x spectrum unrelated to that of the primary ITG instability. A snapshot (at $t = 62.3$) of the instantaneous growth rates of the zonal modes vs k_x is shown in Fig. 2(a). These growth rates increase with the amplitude of the primary mode, $\gamma \propto \phi_l \propto e^{\gamma_l t}$, and, thus, just before nonlinear saturation, $\gamma \gg \gamma_l$. This can be seen from the solid line in Fig. 1(b), which tracks the instantaneous growth rate of the fastest secondary mode in Fig. 2(a) (i.e., $k_x \simeq 0.4$). For comparison, the dashed line in Fig. 1(b) shows $\gamma_\phi = Ck_y|\phi_l|$, where $C = 0.2$ has been chosen to yield $\gamma_\phi = \gamma$ at the time of Fig. 2(a). We obtain $C = 0.3$ below from a simple model.

Motivated by these observations, we focus on the behavior just before saturation, when the secondary modes have small amplitudes compared to the primary, but have growth rates $\gamma \gg \gamma_l$. It is during this phase, in which the finite-k_x

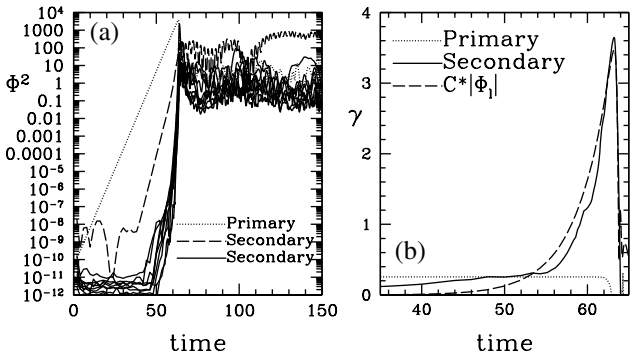

FIG. 1. (a) Mode amplitudes and (b) growth rates vs time

 0031-9007/00/85(25)/5336(4)$15.00

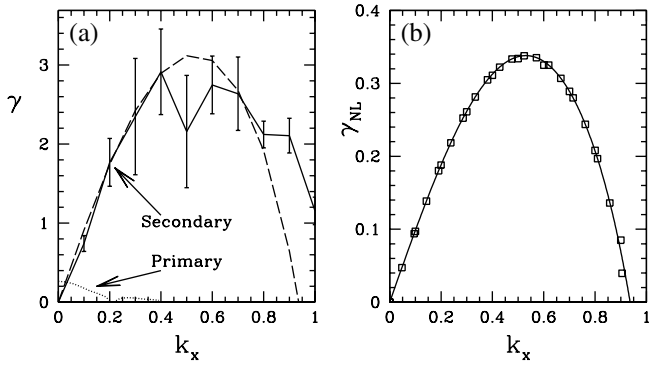

FIG. 2. Secondary mode growth rates vs k_x.

modes grow roughly as the exponential of an exponential, that the bulk of the zonal flow is generated. In this regime the secondary modes can be analyzed in the context of a linear stability analysis, treating the linear ITG mode eigenfunction as a static, quasiequilibrium background. The radial streams associated with this ITG mode background state then drive a Kelvin-Helmholtz–like (KH-like) instability with $\gamma \propto |\phi_l|$, and a k_x spectrum that is in good agreement with the simulations. These KH-like eigenmodes necessarily possess a zonal flow component, and provide a natural nonlinear mechanism through which zonal flows are created throughout the simulation.

Our analysis is based on the electrostatic gyrofluid model with adiabatic electrons [5]. At the time of interest, at which the growth rates of secondary modes exceed $k_\parallel v_{\mathrm{th},i}$ [taking $k_\parallel \sim 1/(qR)$, for example], n and $T_\perp$ decouple from the other moments. The model is further simplified by neglecting the usual linear contributions from the equilibrium magnetic curvature, shear, and background gradients, which are weak compared to the nonlinear driving terms. The resulting equations, dropping terms of order $(k_\perp \rho_i)^4$ compared to unity, are

$$\frac{dn}{dt} + \frac{1}{2}[\tau\nabla_\perp^2\psi, T_\perp] = 0, \qquad \frac{dT_\perp}{dt} = 0, \tag{1}$$

where $d/dt = \partial/\partial t + [\psi, \cdot]$, ψ is the guiding center electrostatic potential, and $n = \psi - \langle\psi\rangle - \nabla_\perp^2[(1+\tau)\psi - \tau\langle\psi\rangle + \tau T_\perp/2]$. Length scales are normalized to ρ_{se}, $\tau = T_{i0}/T_{e0}$, $n = n_{\mathrm{phys}}R/(\rho_{se}n_0)$, $T_\perp = T_{\perp,\mathrm{phys}}R/(\rho_{se}T_{i0})$, and $\psi = e\psi_{\mathrm{phys}}R/(\rho_{se}T_{e0})$. Angle brackets denote a flux surface average, and reduce in the high amplitude (2D) limit to an average over y. We next take $\psi = \psi_l(y) + \tilde{\psi}(y)\exp(\gamma t + ik_x x)$, $T_\perp = T_l(y) + \tilde{T}_\perp(y)\exp(\gamma t + ik_x x)$, where $\psi_l(y)$, $T_l(y)$ represent a periodic configuration of radial streams similar to that produced by the linear ITG mode, e.g., $\psi_l(y) = \psi_{l0}'\sin(k_l y)/k_l$, $T_l(y) = T_{l0}'\sin(k_l y + \delta)/k_l$, for various constants ψ_{l0}', T_{l0}', k_l, and δ. Linearizing in $\tilde{\psi}$, $\tilde{T}_\perp$, and noting $\langle\psi_l\rangle = 0$, one finds

$$-(1+\tau k_x^2)\bar{\gamma}\langle\tilde{\psi}\rangle + [\gamma + k_x^2\Gamma]\tilde{\psi} = \partial_y[\Gamma\bar{\gamma}\partial_y(\tilde{\psi}/\bar{\gamma})], \tag{2}$$

with $\Gamma = \tau\gamma + \bar{\gamma}_T$, $\bar{\gamma} = \gamma - ik_x\psi_l'(y)$, and $\bar{\gamma}_T = \gamma - ik_x[(1+\tau)\psi_l'(y) + \tau T_l'(y)]$. In general, this eigenvalue problem must be solved numerically. In the typical case $k_l^2 \ll 1$ relevant to the simulations, however, an analytical solution for ψ may be obtained as a power series in k_l^2 by treating the right-hand side as small, $O(k_l^2)$. To lowest order, the solution is

$$\tilde{\psi} = \frac{\bar{\gamma}\langle\tilde{\psi}\rangle}{\gamma + f(k_x)\bar{\gamma}_T}, \qquad f(k_x) = \frac{k_x^2}{1+\tau k_x^2}. \tag{3}$$

The (lowest order) dispersion relation follows by integrating this equation over y. Using the identity $\langle\bar{\gamma}/\gamma\rangle = 1$ valid for the periodic case, it may be written as

$$\left\langle \frac{\bar{\gamma}\bar{\gamma}_T}{\gamma + f(k_x)\bar{\gamma}_T} \right\rangle = 0. \tag{4}$$

In the limit $k_x^2 \ll 1$, this reduces to $\langle\bar{\gamma}\bar{\gamma}_T\rangle \simeq 0$. In the usual ITG case that $\psi_l(y)$ ($\simeq \phi_l(y)$ for $k_l \ll 1$) and $T_l(y)$ are $\pi/2$ out of phase, $T_l(y)$ makes no contribution, and one obtains $\gamma = [(1+\tau)/2]^{1/2}|k_x\phi_{l0}'|$ for $\phi_l(y) = \phi_{l0}'\sin(k_l y)/k_l$. This growth rate, $\gamma \sim k_x\phi_{l0}' = k_x V$, is similar to that of the well-known KH instability in the limit $k_x \ll k_l$. For the KH mode, the maximum growth rate $\gamma_{\max} \sim k_l V$ is reached for $k_x \sim k_l$, and stability is obtained for $k_x > k_l$. In the present case, the expansion of Eq. (4) is valid until $k_x \sim 1 \gg k_l$, leading to the much larger growth rate $\gamma_{\max} \sim V$ at $k_x \sim 1$. For example, for $\tau = 0$, one finds $\gamma = k_x\phi_{l0}'[(1-k_x^2)/(2-k_x^4)]^{1/2}$.

For $k_x \sim 1$, the assumption $\tau k_\perp^2 [= (k_\perp\rho_i)^2] \ll 1$ made in deriving Eq. (1) requires $\tau \ll 1$. However, for $k_l \ll 1$, one can easily retain all orders in $k_x\rho_i$. The result, to lowest order in k_l^2, is the same as Eqs. (3) and (4), with the replacements $f(k_x) = (1-\Gamma_0)/\tau$, $\bar{\gamma}_T = \gamma - ik_x\{(1+\tau)\psi_l'(y) + [b\Gamma_0'/(1-\Gamma_0)]\tau T_l'(y)\}$, where $b = \tau k_x^2$, $\Gamma_0(b) = I_0(b)e^{-b}$, $I_0(b) = J_0(ib)$ are the modified Bessel function, and $\Gamma_0' = d\Gamma_0/db$. Again, considering sinusoidal perturbations with $T_l' = 0$, the dispersion relation gives

$$\gamma = \frac{[(1+\tau)/2]^{1/2}[1-(2+\tau)g]}{[1-(2+\tau)g + (1+\tau)g^2/2]^{1/2}}|k_x\phi_{l0}'|, \tag{5}$$

where $g = (1-\Gamma_0)/(\tau + 1 - \Gamma_0)$. Instability is obtained for $(2+\tau)g < 1$, which reduces for $\tau k_x^2 < 1$ to $(1+\tau)k_x^2 (= \rho_s^2 k_x^2) < 1$. This result for $\gamma_{\mathrm{NL}} \equiv \gamma/|\phi_{l0}'|$ is plotted for $\tau = 1$ in Fig. 2(b) (solid line). The data points show the values obtained from a nonlinear gyrokinetic simulation of a 2D radial streamer in the small $k_l \ll 1$ limit, in the absence of curvature and magnetic shear. By applying this result to the parameters $k_l = 0.3$, $k_x = 0.4$ relevant to Fig. 1(b), we obtain $\gamma_\phi = Ck_l|\phi_l|$ with $C \simeq 0.3$.

We now turn to the comparison of our results to work based on the modulational instability [6–11]. Such calculations focus on the excitation of zonal flow by finite amplitude waves (such as drift waves), and are based on truncated Fourier expansions of the secondary mode eigenfunction (e.g., a three-wave interaction). This expansion is valid if the secondary mode has a small complex frequency compared to that of the primary wave. In the present case, for which $\gamma_l \sim \omega_l$, these calculations produce growth rates which are necessarily small compared to γ_l. Here, we have addressed the opposite case of strongly growing secondary modes, $\gamma > \gamma_l$. The eigenfunction we obtain [e.g., Eq. (3)] generally consists of many k_y harmonics of the primary mode. For $k_x \ll 1$ and $k_l \ll 1$, however, the leading order result $\tilde{\phi}(y) \propto \bar{\gamma}$ found here can be represented by a simple expansion of the form $\tilde{\phi}(y) = c_0 + c_+ e^{ik_l y} + c_- e^{-ik_l y}$. Substituting this into Eq. (2) and matching the terms proportional to $e^{\pm ik_l y}$ and those independent of y, and considering $\tau = T_l = 0$, $k_l \ll 1$ for simplicity, yield $\gamma = k_x \phi'_{l0}[(1 - k_x^2)/(2 + 2k_x^2)]^{1/2}$. This is the same as the growth rate obtained in Ref. [11] (well above threshold, for $k_l \ll 1$). Therefore, in the limit of small k_x and k_l, the weak and strong secondary mode approximations yield the same growth rate $\gamma \simeq k_x \phi'_{l0}/\sqrt{2}$. Furthermore, even in the regime $k_x \sim 1$ ($k_l \ll 1$) in which a simple expansion of $\tilde{\phi}$ is not valid, the result of Ref. [11] is qualitatively similar to our result, for $\tau = 0$. This suggests the growth rates found in the context of modulational instability calculations can remain qualitatively reasonable even outside their realm of validity.

The nonlinear evolution of the secondary modes produces a spectrum of zonal flows in the simulations, which ultimately break up the primary ITG streamers. The bulk of these zonal flows then rapidly decays away on a time scale associated with transit-time damping. In a strongly turbulent regime well above the threshold for linear stability, this leads to the reemergence of the linear modes and a complex turbulent cycle. The dynamics of trapped particles in a toroidal geometry also leads, however, to an undamped residual component of the zonal flows [12], that near marginal linear stability is sufficient to nearly suppress further turbulence in the system. We now show that this nonlinear, shear-flow-dominated state is itself subject to instabilities—"tertiary modes"—when the zonal flows exceed a critical threshold. Above this threshold, the tertiary modes are observed to grow to nonlinear amplitudes and damp the zonal flows. The threshold is associated with the boundary of the nonlinear Dimits up-shift.

To illustrate this we examine the fate of small k_y perturbations in a pure zonal flow ($k_y = 0$, $k_x \neq 0$) equilibrium state. This state is obtained from a nonlinear gyrokinetic simulation just above marginal linear stability (i.e., within the nonlinearly suppressed region), evolved out to late times when the system is dominated by the undamped, quasistatic zonal flows. The physics parameters used in this simulation are the same as before, except $R/L_T = 4.75$. The $\mathbf{E} \times \mathbf{B}$ shear in the simulation at late times arises predominantly from an undamped $k_x = 0.25$ component of ϕ, but other wavelength components of ϕ are also present, as are small $k_x \simeq 0.25$ components in $T_\perp$, $T_\parallel$, etc. We then artificially vary the average $\mathbf{E} \times \mathbf{B}$ shearing rate of this quasiequilibrium relative to the rate actually observed in the simulation by a constant rescaling of all of the finite k_x amplitudes. Figure 3(a) shows, as a function of the root-mean-square shearing rate γ_E, the measured growth rate of small $k_y \neq 0$ perturbations maximized over all k_y values. For $\gamma_E = 0$ (the usual linear case), the growth rate in the figure represents an ordinary ITG mode. This mode becomes progressively more stable as γ_E is increased, until absolute stability is attained at $\gamma_E = 0.13$. The actual (i.e., nonscaled) γ_E value of the simulation falls in this stable range, consistent with its nonturbulent behavior at late times. As γ_E is increased further, however, a new instability sets in, with a growth rate that increases monotonically with the shear-flow amplitude. This mode is localized to a spatial region in which the $\mathbf{E} \times \mathbf{B}$ shear is weak (an extremum of V_{Ey}), and propagates with the local $\mathbf{E} \times \mathbf{B}$ velocity at that location, $\omega \simeq k_y V_{Ey}$ with $k_y \simeq 0.7$. Before turning to a discussion of this new mode, we first make the important observation that the stability window seen in Fig. 3(a) does not exist for all parameters. Figure 3(b) shows the corresponding curve obtained at a larger value $R/L_T = 5.75$, in a region of parameter space in which nonlinear simulations display steady turbulence. At this value of R/L_T, the nonlinear suppression of turbulence is impossible because the zonal flows become unstable before the primary ITG mode can be shear-flow stabilized.

To understand this, we consider a linear stability analysis of a shear-flow-dominated, x-dependent state such as that found in the simulation. Near the onset threshold at $\gamma_E \simeq 0.3$ of Fig. 3(a), simulations show that the tertiary mode's growth rate is sensitive to many factors, including the magnetic shear, toroidal curvature, and the background gradients of both $T_\parallel$ and $T_\perp$. We defer discussion of this complicated but physically important threshold regime, and first focus on the opposite limit in which the shear-flow amplitudes associated with the quasiequilibrium state become large. In that limit, as discussed

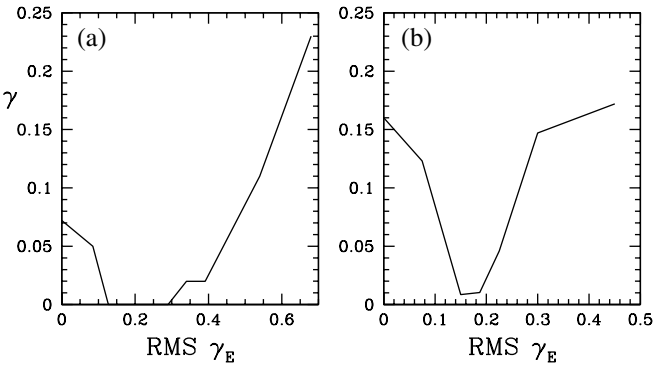

FIG. 3. Growth rates vs RMS γ_E for (a) $R/L_T = 4.75$ and (b) $R/L_T = 5.75$.

earlier, the equations for n and $T_\perp$ (assuming fixed $k_\parallel$) decouple, and the contributions of the magnetic shear, curvature, and background gradients become weak. This is consistent with the simulations, which show that the growth rate at large γ_E does not change if these effects are switched off. We therefore return to Eq. (1), and consider $\psi = \psi_0(x) + \tilde{\psi}(x)\exp(\gamma t + ik_y y)$, $T_\perp = T_0(x) + \tilde{T}_\perp(x)\exp(\gamma t + ik_y y)$, where $\psi_0(x)$, $T_0(x)$ now represent the static, x-dependent zonal flow background state. Linearizing in $\tilde{\psi}$,$\tilde{T}_\perp$, and noting $\langle\psi\rangle = \psi_0$, we obtain

$$[(1 + (1 + \tau)k_x^2)\bar{\gamma} + ik_y(k_y^2\tau T_0' - \tau\psi_0''')]\tilde{\psi} = \partial_x[(\tau\gamma + \bar{\gamma}_T)\bar{\gamma}\partial_x(\tilde{\psi}/\bar{\gamma})], \quad (6)$$

with $\bar{\gamma} = \gamma + ik_y\psi_0'(x)$, $\bar{\gamma}_T = \gamma + ik_y[(1 + \tau)\psi_0'(x) + \tau T_0'(x)]$. As noted earlier, the zonal flow state generated by the simulation on which Fig. 3 is based is dominated by a single $k_x \simeq 0.25$ mode in $\psi(x)$. A smaller $k_x \simeq 0.25$ component in the ion temperature $T_0(x)$, π out of phase with that in $\psi_0(x)$, is also observed. This behavior is generic, in the sense that such an undamped state emerges at late times from the simulations across a broad range of parameters and initial conditions. It is also consistent with an analysis [13] based on the formalism of Ref. [12]. In view of our earlier results, one might expect that the small contribution from $T_0(x)$ in Eq. (6) could be neglected compared to that in ψ_0, but this is not the case. The simulations show that the instability at large γ_E depends critically on the presence of both ψ_0 and T_0. This behavior is in agreement with our numerical study of Eq. (6), which predicts an instability very similar to that observed in the simulations. This instability is radially localized to the regions where the shearing rate $\propto \psi_0''$ vanishes, corresponding to extrema in both ψ_0' and T_0', and has a frequency $\omega \simeq -k_y\psi_0'$ ($\bar{\gamma} \simeq 0$). Upon expanding Eq. (6) about $x = x_0$ (where $\psi_0'' = T_0'' = 0$) and defining $\lambda = (2\tau T_0'/\psi_0''')^{1/4}|_{x_0}$ (where $T_0'/\psi_0''' > 0$ by virtue of the phase relationship between T_0 and ψ_0), a simple scaling of the growth rate is obtained in the limit $k_x \ll 1$, in which $\lambda(\propto k_x^{-1/2}) \gg 1$. In this case, λ is found to represent the radial scale of the mode, and one obtains a maximum growth rate $\gamma \simeq 0.55k_y\sqrt{\tau T_0'\psi_0'''/2}$ for $k_y \simeq 1/\lambda$ in good agreement with the simulations.

At the more modest zonal flow amplitudes $\gamma_E \sim 1$ characteristic of the threshold region in Fig. 3, the behavior of the instability predicted by our gyrofluid analysis and observed in the gyrokinetic simulations is substantially more complicated. The addition of the realistic background equilibrium gradients in $T_\perp$ and n_0 overpowers the $k_x \simeq 0.25$ contribution to T_0' just discussed, and the magnetic shear leads to an absolute stability threshold at $\gamma_E \sim 1$. At finite $\hat{s}$, the addition of an equilibrium parallel temperature gradient in the system excites a linear slab ITG instability, which in turn is suppressed by the introduction of the magnetic curvature. One clear dependence of the stability threshold on the parameters, however, has been extracted: increasing q in the runs of Fig. 3 from $q = 1.4$ to $q = 3$ essentially eliminates the nonlinear Dimits up-shift. This result is consistent with the stabilizing role of finite $k_\parallel \propto 1/q$, which acts on both the nonlinear zonal flow instability as well as the primary ITG mode. At higher q values both modes become more unstable, thus closing the stability window seen in Fig. 3(a).

In summary, we have carried out two stability studies relevant to zonal flow dynamics in collisionless plasma. The first addresses the stability of radial streamers, such as those generated by an unstable ITG mode. We find these excite strong KH-like modes at $k_\perp\rho_s \lesssim 1$, which act to break up the primary mode and lead to the production of zonal flows. The second study addresses, using the same formalism, the stability of these zonal flows. The nature of the adiabatic electron response leads to very different behavior in this case. The KH modes arising in the radial streamer problem are no longer present, and the dominant instabilities in the system are much weaker. These modes require a finite gradient of $T_\perp$ to be unstable, and are localized to regions where the $\mathbf{E} \times \mathbf{B}$ shearing rate of the zonal flows is small. They exhibit growth rates that increase with the average shearing rate, and are stable when γ_E falls below a critical level. Near marginal stability of the primary linear modes, shearing rates somewhat below this critical level can be sufficient to stabilize the system to all modes, leading to the phenomenon of the nonlinear Dimits up-shift.

[1] W. Dorland, Ph.D. thesis, Princeton University, 1993; G. W. Hammett *et al.,* Plasma Phys. Controlled Fusion **35**, 973 (1993); R. E. Waltz *et al.,* Phys. Plasmas **1**, 2229 (1994); M. A. Beer, Ph.D. thesis, Princeton University, 1995; A. M. Dimits *et al.,* Phys. Rev. Lett. **77**, 71 (1996).
[2] Z. Lin *et al.,* Science **281**, 1835 (1998).
[3] A. M. Dimits *et al.,* Phys. Plasmas **7**, 969 (2000).
[4] M. Beer *et al.,* Phys. Plasmas **2**, 2687 (1995).
[5] W. Dorland and G. Hammett, Phys. Plasmas **5**, 812 (1993)
[6] J. Drake *et al.,* Phys. Fluids B **4** (1992).
[7] P. N. Guzdar, Phys. Plasmas **2**, 4174 (1995).
[8] V. B. Lebedev *et al.,* Phys. Plasmas **2**, 4420 (1995).
[9] P. H. Diamond *et al.,* in Proceedings of the 17th IAEA FEC, 1998 (to be published).
[10] L. Chen *et al.,* Phys. Plasmas (to be published).
[11] P. N. Guzdar *et al.* "Shear Flow Generation by Drift Waves Revisited" (to be published).
[12] M. N. Rosenbluth and F. Hinton, Phys. Rev. Lett. **80**, 724 (1998).
[13] G. W. Hammett (private communication).